Effect of the Precise Branching of Polyethylene at Each 21st CH_2 Group on Its Phase Transitions, Crystal Structure, and Morphology

Wulin Qiu,[†,‡] John Sworen,[§,⊥] Marek Pyda,[†,‡] Elisabieta Nowak-Pyda,[†] Anton Habenschuss,[‡] Kenneth B. Wagener,[§] and Bernhard Wunderlich*[,†,‡]

Department of Chemistry, The University of Tennessee, Knoxville, Tennessee 37996-1600; Chemical Sciences Division, Oak Ridge National Lab., Oak Ridge, Tennessee 37831-6197; Center for Macromolecular Science & Engineering, Department of Chemistry, University of Florida, Gainesville, Florida 32611; and DuPont Research & Development, Jackson Laboratory, Deepwater, New Jersey 08023

Received September 15, 2005; Revised Manuscript Received October 23, 2005

ABSTRACT: Three linear polyethylenes with branches at every 21st backbone atom have been analyzed by differential scanning calorimetry (DSC) and quasi-isothermal, temperature-modulated DSC. The branches were methyl (PE1M), dimethyl (PE2M), and ethyl groups (PE1E). Linear polyethylene (HDPE) and atactic poly(octadecyl acrylate) (PODA) were also analyzed. All were compared to a random poly(ethylene-*co*-octene-1) of similar branch concentration (LLDPE) and poly(4,4′-phthaloimidobenzoyldoeicosyleneoxycarbonyl) (PEIM-22). The HDPE has the highest melting temperature and crystallinity with relatively large contributions of reversing melting when grown as folded-chain crystals. The precisely branched polyethylenes and copolymers have lower melting temperatures and heats of fusion. Of the branched samples, PE1M crystallizes more readily, followed by PE1E and PE2M, with PE2M showing cold crystallization. In contrast to paraffins of equal length which melt fully reversibly, the precisely designed, branched polymers melt largely irreversibly with small amounts of reversing melting, which is least for the best-grown crystals. The PE1M forms monoclinic, PE1E, pseudohexagonal, or triclinic crystals, and PE2M has a multitude of crystal structures.

1. Introduction

In addition to molar mass, polydispersity, and thermal and mechanical history, the thermal properties of polymers are influenced by their chemical microstructure.[1] Different polyethylenes, PEs, the most studied flexible, linear macromolecules, can be described as follows: PM, polymethylene, a pure high-molar-mass polymer made from diazomethane; HDPE, a high-density PE with few long-chain branches, produced at low ethylene pressure by cationic or coordination polymerization; LDPE, a low-density PE made at high ethylene pressure via free-radical processes and containing mainly short, random branches of four and five carbon atoms; and LLDPE, a linear-low-density PE, which is made by copolymerization with monomers such as 1-octene, 1-hexene, or 1-butene. The random LLDPE copolymer, when made by multiple-site, heterogeneous coordination catalysts, has a wide variations in copolymer content between the molecules.[2] More modern LLDPEs are produced by single-site, homogeneous metallocene catalysts and produce randomly distributed comonomer units along the chain with similar concentrations in all molecules.[3]

Polyethylenes with precisely spaced, identical branches were synthesized most recently via acyclic diene metathesis, ADMET,[4] and are featured in this research and compared to other PEs and model compounds. Three such linear polyethylene samples were analyzed. Their branches were at every 21st backbone atom: PE1M with single methyl groups, PE2M with dimethyl groups, and PE1E with ethyl groups. For comparison, poly(octadecyl acrylate), PODA, with side chains of $-(CO)-O(-CH_2)_{17}-CH_3$, and an HDPE, identical to a previously widely studied sample,[5−7] have been newly analyzed. The earlier analyzed metallocene-catalyzed copolymers with 1-octene, LLDPE, with a similar branch concentrations were used as a model compounds,[8−10] and poly(4,4′-phthaloimidobenzoyldoeicosyleneoxycarbonyl), PEIM-22, with $(CH_2-)_{22}$ sequences was used for comparison in the Discussion. The structures of five of these compounds are shown in Figure 1.

A large number of thermal analyses on melting and crystallization of the various PEs can be found in the literature. The first adiabatic calorimetry on LDPE of 50−55% crystallinity[11] and HDPE of 83 and 93% crystallinity[12] was done about 50 years ago. Since then, the glass transition ($T_g = 237$ K, $\Delta C_p = 10.5$ J K^{-1} mol^{-1}),[13] equilibrium melting of orthorhombic PE ($T_m^\circ = 414.6$ K, $\Delta H_f = 4.11$ kJ mol^{-1}),[14] and thermodynamic functions C_p, H, S, and G for crystalline, liquid, and glassy PE were established, based on over 100 measurements made in different laboratories.[15] The link of the thermal properties to the density of vibrational states was also evaluated.[16−18] This effort established the equilibrium thermodynamic properties of PE to a degree comparable to the best-characterized small molecules. Extended-chain crystals of close to 100% crystallinity could also be studied directly with differential scanning calorimetry (DSC) and used in the analysis of the thermodynamic heat capacity and equilibrium melting temperature.[19,20] The phase diagram of PE of broad molar mass distribution was determined on the basis of equilibrium thermodynamics.[5,7] Even the nonequilibrium properties, such as incomplete crystallization, crystal and molecular nucleation, cold crystallization, annealing, recrystallization, crystal perfection, superheating, broadening of the glass transition on partial crystallization, and the properties of oriented, more or less rigid-amorphous nanophases could be assessed by introducing time-dependent calorimetry.[1]

† The University of Tennessee.
‡ Oak Ridge National Lab.
§ University of Florida.
⊥ Jackson Laboratory.
* Corresponding author: E-mail: Wunderlich@CharterTN.net.

10.1021/ma052010w CCC: $33.50
Published on Web 11/24/2005

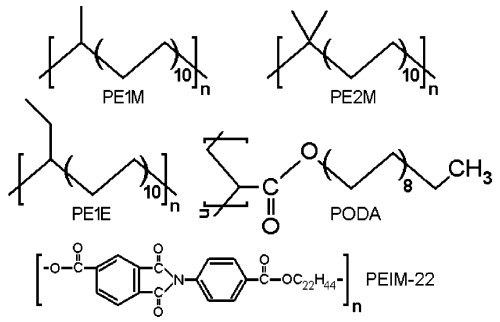

Figure 1. Chemical structure of the analyzed PE1M, PE2M, PE1E, PODA, and PEIM-22.

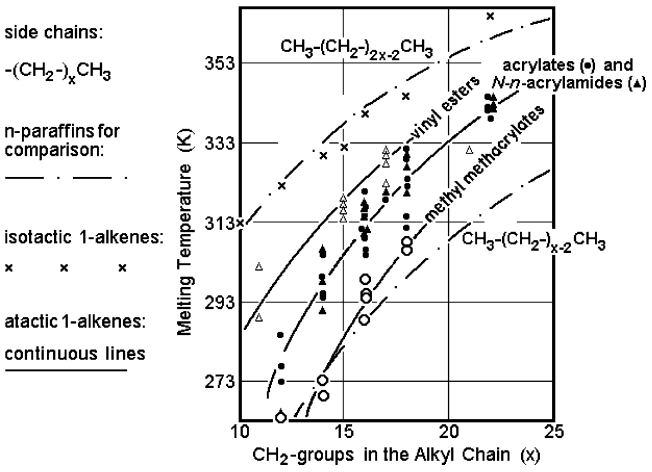

Figure 2. Melting temperatures of a number of different atactic vinyl polymers with long *n*-paraffinic side chains. The melting points change between those of *n*-paraffins of the same to twice the side-chain length.[26]

The distinction between equilibrium and irreversible thermodynamics has recently been studied more efficiently by temperature-modulated differential scanning calorimetry (TMDSC) in its quasi-isothermal mode.[21,22] The quasi-isothermal mode of TMDSC consists of a long-time temperature modulation of 0.1−2.0 K with periods of 20−100 s about a constant temperature, T_0. Measurement commences in such TMDSC after all irreversible processes have become immeasurable, usually after 10 min, but sometimes after several hours. A major result from these observations is that it is necessary to introduce variable points of decoupling of molecular segments at the phase boundary and possibly even at entanglements. This gives the decoupled segments of the molecule different properties.[23] Locally reversible melting within the metastable, semicrystalline polymers is one of the processes involving decoupling at the crystal growth face.[24]

Classical thermodynamics[25] treats the macromolecule either as a whole, when, for example, colligative properties are to be described, or as an assembly of decoupled repeating units, when, for example, copolymer melting is to be described. Neither alternative is able to describe the reversible melting discovered by TMDSC. Decoupling is to be tested in this research using the molecules of Figure 1. It is to be investigated if the segments of 20 CH_2 groups are long enough to form nanocrystals of their own, separated from noncrystalline layers, or if they are included within larger crystals. Decoupling was assumed earlier on discussing polymers with *n*-paraffinic side chains which have melting temperatures, T_m, similar to corresponding paraffins, as shown in Figure 2.[26]

To conclude the Introduction, a short summary of recent results by TMDSC on PE, its oligomers, and paraffins is given to support the Discussion, below. For *n*-paraffins up to $C_{60}H_{122}$, which grow as extended-chain crystals, quasi-isothermal TMDSC proved no supercooling and a reversible melting.[27] Paraffin crystal nucleation was shown to be possible on surfaces that are frequently present in such experiments.[28] Also, there is little difference in reversibility between pure paraffins and polyethylene fractions of similar average mass,[29] except for the need to demix on crystallization, as required by the eutectic phase diagram.[1] Folded-chain crystals are only observed at longer chain length.[30] Extended-chain crystals of PE of high molar mass show practically no reversible melting,[7] while PE with many folds shows some reversible melting on the lateral surfaces.[24] Such reversible melting was also seen for gel-spun PE of ultrahigh molar mass[31] and to a larger degree in LLDPE.[8−10] The reversible melting measured by quasi-isothermal TMDSC originates from melting and crystallization of locally decoupled segments of polymer chains.[32]

2. Experimental Section

2.1. Materials. The polyethylenes with precisely controlled chemical microstructure, as displayed in Figure 1, had a respective mass-average molar mass and polydispersity of 20 200 Da and 1.7 for PE1M, 76 000 Da and 1.8 for PE2M, and 37 000 Da and 2.0 for PE1E. The measured glass transition temperatures, T_g, were reported in the temperature range from 230 to 250 K.[4] A sample of HDPE was analyzed for comparison; its mass average was 153 000 Da and polydispersity 18. This polymer was the basis for an earlier extensive analysis (Marlex 50, sample A).[5−7] Previously analyzed LLDPEs, poly(ethylene-*co*-octene), will be discussed also.[8−10] These samples have a 14.2−38.4 wt % (2.0−6.7 mol %) of branches. Sample 2, which was analyzed with TMDSC, had a molar mass of 78 000 Da. Its comonomer concentration is 34.5 wt % (5.8 mol %) and will be compared to the 4.8 mol % branches of samples PE1M, PE1E, and PE2M (for the last, the two $-CH_3$ groups on one carbon atom are counted as one center-connected branch). Poly(octadecyl acrylate), PODA (37 900 Da, polydispersity of 2.5), was purchased from Aldrich Chemical Co. The molar masses of PE1E and PODA were newly measured in the Polymer Characterization Laboratory of the University of Tennessee by size-exclusion chromatography. The PODA had a bimodal distribution with maxima at 47 000 and 6100 Da, giving rise to the larger polydispersity.

2.2. DSC and TMDSC measurements. All new measurements of the apparent heat capacities displayed in Figures 4−6 and 8 were carried out with a Thermal Analyst 2920 system from TA Instruments, Inc. To extend the measurements to safely discuss the beginning of the glass transition of the PEs with the controlled chemical microstructures, a Mettler Toledo DSC 820, capable of liquid nitrogen quenching, was used in the standard DSC mode. Since even such quenching does not produce amorphous samples, the polymers show a broadened glass transition to higher temperature, as is common in semicrystalline polymers. No detailed traces of the Mettler Toledo DSC are displayed since they only extend the shown curves to somewhat lower temperature. The calibration and measurements were carried out analogous as for the Thermal Analyst 2920, described next. Both calorimeters are isoperibol, heat-flux, twin calorimeters, capable of standard and temperature-modulated operation.[1] The data on LLDPE in Figure 7 were gained earlier in our laboratory using a power-compensation Perkin-Elmer DSC 7, again under comparable conditions. Details on these measurements were described earlier.[9,10]

Temperature measurement and control of modulation within the Thermal Analyst 2920 are by the sensor of the sample temperature. During the experiments, a refrigerated cooling system with a cooling capacity to 220 K was used, and a dry N_2 gas with a flow rate of 25 mL min^{-1} was purged through the DSC cell. The temperature was calibrated in the standard DSC mode, using the onset temperature of the melting transition for indium at 429.75 K. The heat-flow rate was precalibrated with the specific heat of fusion of

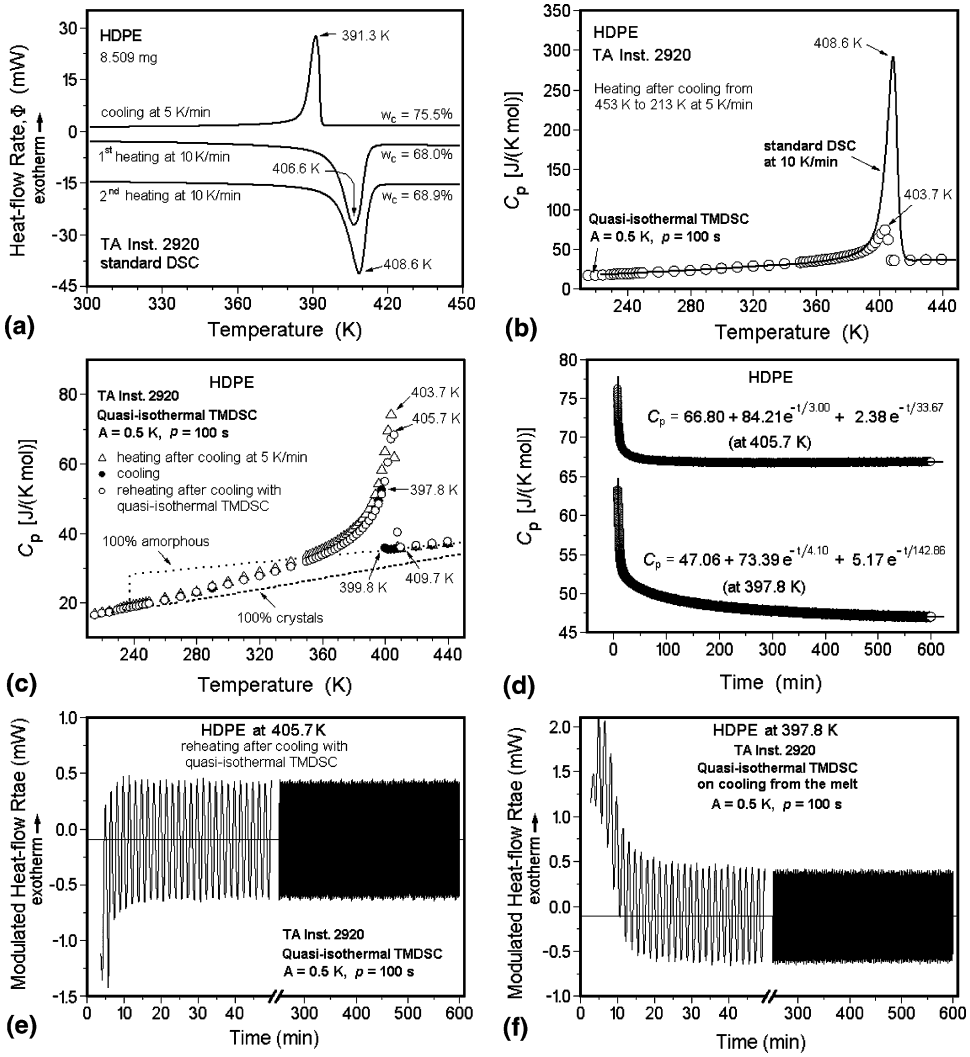

Figure 3. Results for HDPE on standard DSC and quasi-isothermal TMDSC on heating, cooling, and reheating: (a) standard DSC traces; (b) comparison of C_p by standard DSC and quasi-isothermal TMDSC on heating after cooling at 5 K min^{-1} from the melt; (c) apparent, reversing C_p on stepwise heating, cooling, and reheating, measured by quasi-isothermal TMDSC; (d) time dependence of the apparent C_p on long-time quasi-isothermal analysis at 405.7 and 397.8 K (see see reheating and cooling runs in (c)); (e, f) time-domain recordings of Φ corresponding to (d).

indium (28.62 J g^{-1})[33] at a scanning rate of 10 K min^{-1}. The melting temperature of indium was also measured in the quasi-isothermal mode with a 0.5 K temperature amplitude after the calibration in the standard mode to identify any differences between the two modes of measurement. It was found that quasi-isothermal TMDSC experiments after initial standard DSC calibration led to a lower melting temperature of 428.89 K, somewhat different from the expected extrapolation from 10 K min^{-1} to zero heating rate (429.44 K). To correct the sample temperatures from quasi-isothermal TMDSC, 0.86 K were added to the average temperatures of the quasi-isothermal measurements.

In all experiments, standard aluminum pans of 20 μL volume with covers were used for the sample and as empty reference. Three runs were carried out for the quantitative measurements: (1) sapphire vs empty reference pan, (2) empty pan vs empty reference pan, and (3) sample vs empty reference pan. A somewhat lighter reference pan was fixed for all measurements to establish a known phase shift to appropriately correct for the asymmetry of the calorimeter.[34] The standard DSC was performed at 10 K min^{-1} from 213 to 453 K with a 10 min isotherm at the beginning and end. A fresh PE sample (as delivered) was used in the first heating run, followed by cooling at 5 K min^{-1}, and a second heating run at 10 K min^{-1}.

The quasi-isothermal TMDSC was performed using sinusoidal modulation about successive base temperatures, T_0, with a modulation period of $p = 100$ s, a modulation amplitude of $A_{T_s} = 0.5$ K, and stepwise temperature changes in T_0 of 2−30 K, depending on the changes anticipated in the sample response. The last 10 of the 20 min quasi-isothermal runs were used for data collection to calculate the reversing c_p as

$$mc_p = \frac{A_\Phi}{A_{T_s}\omega}\sqrt{1+\tau^2\omega^2} \qquad (1)$$

where m is the sample mass, c_p is the specific heat capacity in J K^{-1} g^{-1}, and A stands for the respective modulation amplitudes. Note that $A_{T_s}\omega$ is the amplitude of the heating rate for a sinusoidal modulation with frequency ω ($= 2\pi/p$, where p is the period in s). If the modulation amplitude is not sinusoidal, a Fourier transformation into the various harmonics is made, and eq 1 applies then to the chosen harmonic (usually the first). The second term in eq 1 contains the calibration factor τ and accounts for the effect of different measuring frequencies. The values of τ are usually evaluated empirically by separate runs.[1]

For some samples a standard DSC trace at 10 K min^{-1} was run immediately after the completion of the slow, stepwise cooling of the quasi-isothermal TMDSC to measure the crystallinity of the, thus, annealed samples. Unless otherwise stated, the crystallinity, w_c, shown in the figures was calculated from the basic equation

$$dH = \left(\frac{\partial H}{\partial T}\right)_{p,n} dT + \left(\frac{\partial H}{\partial n}\right)_{p,T} dn \qquad (2)$$

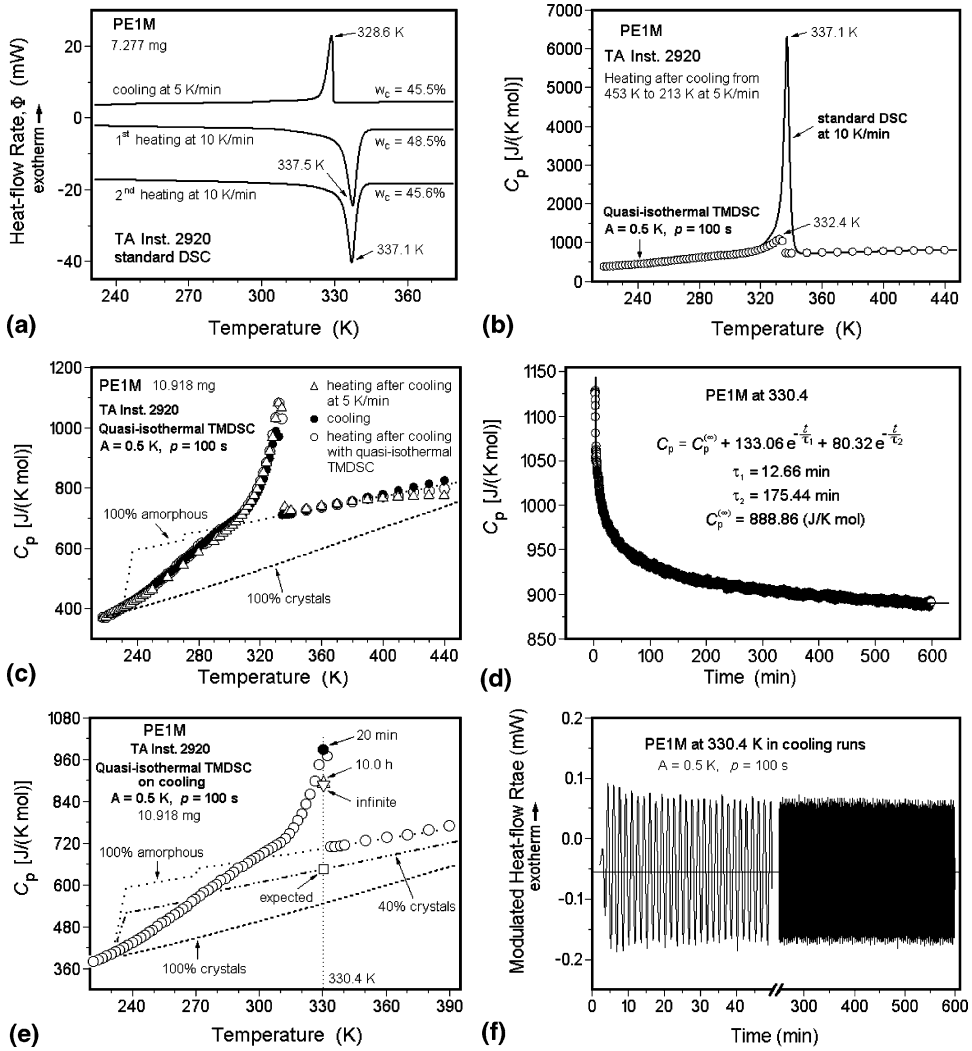

Figure 4. Results for PE1M on standard DSC and quasi-isothermal TMDSC on heating, cooling, and reheating: (a) standard DSC traces; (b) comparison of C_p by standard DSC and quasi-isothermal TMDSC on heating after cooling at 5 K min^{-1} from the melt; (c) apparent, reversing C_p on stepwise heating, cooling, and reheating, measured by quasi-isothermal TMDSC; (d, e) time dependence of the apparent C_p on long-time quasi-isothermal analysis on the cooling run of (c); (f) time-domain recordings of Φ corresponding to (d).

the equation which expresses the differential change in enthalpy as the sum of the heat capacity $(\partial H/\partial T)_{p,n}$ dT and the latent heat $(\partial H/\partial n)_{p,T}$ dn, where the subscripts p, n, and T indicate the constancy of p, n, and T. The measured heat of fusion, ΔH, is the excess above the thermodynamic heat capacity, integrated over temperature, so that the crystallinity is $w_c = (\Delta H/\Delta H_f)$. The heat of fusion of 100% orthorhombic crystalline PE, ΔH_f, is 293.0 J g^{-1} (4.11 kJ mol^{-1}) at the equilibrium melting temperature of 414.6 K.[14] For all crystallinity calculations, ΔH_f of the orthorhombic PE was used at the temperature of the respective melting peak. Deviations due to different crystal structures are addressed in the Discussion. It should be noted that C_p is an abbreviation for heat capacity. If necessary, different C_ps, such as reversing C_p, total C_p, etc., and theoretical quantities, such as thermodynamic C_p and excess C_p, are identified by the appropriate adjective.

2.3. WAXD Measurements. The X-ray experiments were performed in the Central X-ray Facility of UTK on samples of varying thickness. The diffractometer was a Philips X'Pert X-ray unit, working in reflection geometry using Cu Kα radiation (0.1542 nm), operated at 40 kV and 45 mA. The fresh samples were used, and all measurements were done at room temperature in air. Data in the range of $2\theta = 5-40°$ were collected at scan steps of 0.05°.

3. Results

3.1. HDPE. Figure 3 shows the results of standard DSC and quasi-isothermal TMDSC of HDPE. The melting temperatures, T_m, obtained by standard DSC in Figure 3a are much lower than the equilibrium melting temperature of the sample (414.0 K)[5] but agree with earlier results.[35]

The quasi-isothermal TMDSC experiments in Figure 3b exhibit only a small peak in the reversing C_p when compared to the standard DSC. The reversing melting peak is narrower and is located inside the melting peak of the standard DSC trace. The peak-heights of the apparent C_p above the baseline of the liquid sample are 256 J K^{-1} mol^{-1} at 408.6 K by DSC and 39 J K^{-1} mol^{-1} at 403.7 K by TMDSC. Figure 3c contains an enlarged plot of same reversing C_p, together with the results gained on cooling and on repeating the quasi-isothermal experiment on heating after the prior cooling run. The dotted line is the baseline C_p of the 100% amorphous sample, while the dashed line is the baseline of the 100% vibrational C_p, both as given in the ATHAS Data Bank.[36] The reversing C_p after cooling at 5 K min^{-1} is higher than that on the slow quasi-isothermal cooling and reheating. The quasi-isothermal steps on cooling show a reversing crystallization peak at 397.8 K and an onset of crystallization at 399.8 K. The subsequent heating reveals a reversing melting peak at 405.7 K with the end of melting at 409.7 K. Thus, the experimental supercooling of HDPE is 10 K, as expected from the earlier analyses.[29,35] Long-time modulation experiments give a continuing change

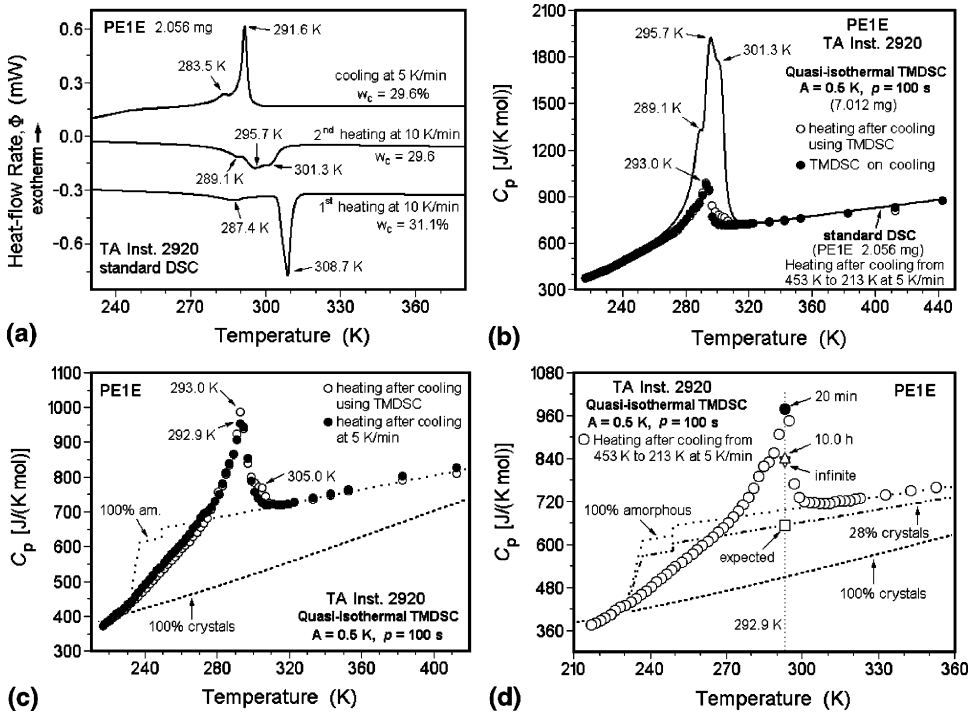

Figure 5. Results for PE1E on standard DSC and quasi-isothermal TMDSC on heating, cooling, and reheating: (a) standard DSC traces; (b) comparison of C_p by standard DSC and quasi-isothermal TMDSC on heating after cooling at 5 K min^{-1} from the melt and followed by cooling; (c) apparent, reversing C_p on stepwise heating and reheating, measured by quasi-isothermal TMDSC; (d) time dependence of the apparent C_p on long-time quasi-isothermal analysis at the maximum of the cooling run of (b).

in the apparent heat capacity as analyzed in Figure 3d. The upper curve (at 405.7 K) shows the variation of C_p at the peak temperature on heating in Figure 3c, while the lower one (at 397.8 K) is at the peak temperature on cooling. A double-exponential fit of the data indicates an ultimately constant level of reversing heat capacity, which is considered to be the reversible melting.[24] These reversible C_ps at 405.7 and 397.8 K are still higher by about 90% and 30%, respectively, than the expected thermodynamic C_p for the appropriate crystallinity. The apparent reversible C_p is also considerably higher than C_p for the liquid. The reversing C_p measured on heating decreases faster than on cooling.

More information on the time dependence of the heat-flow rates, Φ, is gained from Figure 3e,f. In the beginning, the modulated portion of Φ is superimposed on the remaining irreversible melting (lasting about 20 min) and crystallization (lasting about 40 min). Both start on the change of temperature to the chosen T_0. In the heating run of Figure 3e, the shallow maximum in the peaks of the heat-flow rate at 10−12 min is the result of an excess exotherm and is expected from reorganization or recrystallization of some of the crystals. If this produces any crystals with a higher T_m than is reached by the next melting cycle, they do not participate in further melting and recrystallization. After several hundred modulation cycles, a locally reversible melting process is reached.[24] In the cooling run at 397.8 K of Figure 3f the modulation is almost symmetric after about 8 min. A continued small decrease in amplitude is due to reorganization with a relaxation time of about 140 min and is superimposed on the irreversible crystallization without a maximum.

3.2. PE1M. Figure 4 displays the results of standard DSC and TMDSC on PE1M. As described in the Experimental Section, the crystallinities for PE1M listed in Figure 4a and of all subsequent samples have been computed using the heat of fusion of the orthorhombic PE at the given peak temperature and serve only as a comparison to the heat of fusion of PE and for the calculation of the baselines for the C_p of the semicrystalline samples. It is shown in section 3.7 that these polymers do *not* have an orthorhombic crystal structure as seen in PE.

Figure 4b is a comparison of the standard DSC with the quasi-isothermal TMDSC results (circles) on heating after cooling at 5 K min^{-1}. A small, reversing melting peak at 332.4 K on heating is located inside the melting peak of the standard DSC trace. The peak height of the apparent C_p above the baseline of the amorphous sample reaches 5600 J K^{-1} mol^{-1} at 337.1 K in standard DSC, compared to 375 J K^{-1} mol^{-1} at 332.4 K in TMDSC.

Figure 4c contains an enlarged plot of the same reversing C_p, together with the results gained on cooling and on repeating the quasi-isothermal heating experiment after the prior cooling run. The dotted line is the baseline C_p of the 100% amorphous sample, while the dashed line is the heat capacity for 100% crystalline PE1M without latent heat contributions. They were calculated with eq 3 assuming simple additivity of the C_p of two chemical groups in PE1M (see Figure 1):

$$C_p(\text{PE1M}) = 19C_p(\text{PE}) + C_p(\text{PP}) \qquad (3)$$

where C_p(PP) and C_p(PE) are the heat capacities for the appropriate amorphous or crystalline polypropylene, PP ($-CHCH_3-CH_2$), and polyethylene, PE ($-CH_2$), all listed in the ATHAS Data Bank.[36] The cooling run has a crystallization peak at 330.4 K and an onset of crystallization at 334.4 K. On reheating after the TMDSC cooling runs, the major reversing melting peak is at 332.4 K and the end of melting at 336.4 K, which agrees with a published value of 333 K for the peak temperature by DSC extrapolated to zero heating rate.[37] The reversing C_p is similar for all three runs. It is to be noted that the supercooling for crystallization from the melt is only 2 K.

Long-time modulation experiments for PE1M are illustrated in Figure 4d for 330.4 K, the peak temperature on cooling. This run occurred after major crystallization in the prior run (see

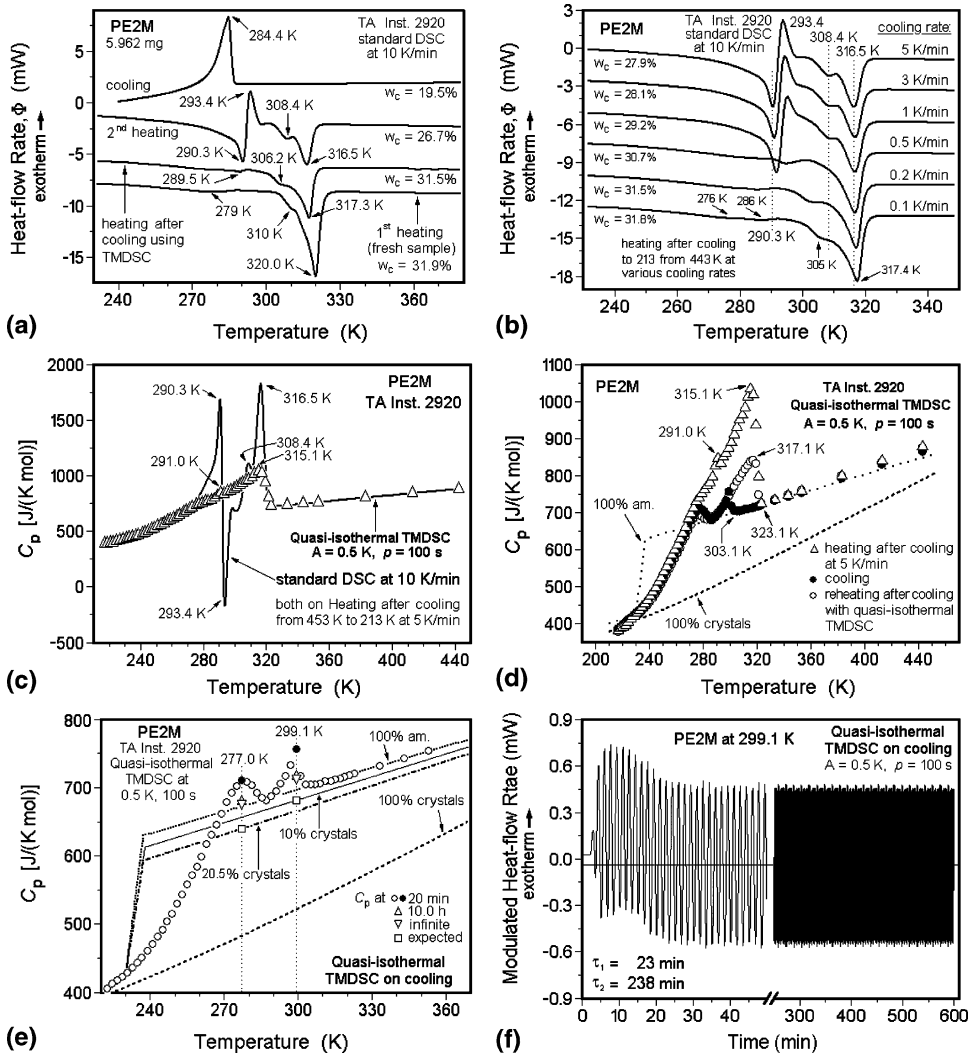

Figure 6. Results for PE2M on standard DSC and quasi-isothermal TMDSC on heating, cooling, and reheating: (a, b) standard DSC traces; (c) comparison of C_p by standard DSC and quasi-isothermal TMDSC on heating after cooling at 5 K min^{-1} from the melt; (d) apparent, reversing C_p on stepwise heating, cooling, and reheating, measured by quasi-isothermal TMDSC; (e) time dependence of the apparent C_p on long-time quasi-isothermal analysis on the cooling-run of (d); (f) time-domain recordings of Φ corresponding to (e).

Figure 4e). The result of a double-exponential fit of the data indicates the ultimately constant level of reversible C_p, also shown in Figure 4e. It is still much higher than the expected value for the remaining crystallinity and is also considerably higher than is known for the 100% amorphous sample. The heat-flow rates plotted in the time domain are given in Figure 4f. The initial heat-flow-rate exotherms decrease more when compared to the endotherms. The decrease in the apparent heat capacity, thus, is mainly due to crystal perfection, in contrast to the analyses in Figures 3f and 6f.

3.3. PE1E. Figure 5 illustrates the standard DSC and quasi-isothermal TMDSC of PE1E. Figure 5a displays the heat-flow rates of the standard DSC with the marked peak temperatures of crystallization and melting. Figure 5b contains a comparison of the quasi-isothermal TMDSC results on cooling from the melt and on subsequent heating to the data from standard DSC on heating after cooling from the melt at 5 K min^{-1}. The matching TMDSC of a sample cooled at 5 K min^{-1} is similar to the heating run in Figure 5b, as is shown in Figure 5c. The reversing melting peak is smaller and narrower than the standard DSC peak. The quasi-isothermal, reversing C_p on cooling in Figure 5b reaches practically the same melting peak as in the heating experiments. The peak heights of the apparent C_p above the baseline of the amorphous are 1225 J K^{-1} mol^{-1} at 295.7 K for standard DSC and 256 J K^{-1} mol^{-1} at 293.0 K for TMDSC.

The baselines indicating the C_p of the liquid and the solid samples were calculated with

$$C_p(\text{PE1E}) = 19C_p(\text{PE}) + C_p(\text{PB}) \qquad (4)$$

where C_p(PE) and C_p(PB) are the C_p of PE and poly-1-butene, PB ($-CHC_2H_5-CH_2$), in the appropriate state, obtained from the ATHAS Data Bank.[36] On heating after cooling using TMDSC, PE1E reveals a major reversing melting peak at 293.0 K as well as a broad shoulder at 305.0 K. The end of the reversing melting peak is at 309.0 K. In TMDSC on cooling and subsequent heating, the reversing peak appears at the same temperature (292.9 K). The onset of crystallization in Figure 5b is at 301.0 K, a supercooling of about 8 K, more than for PE1M but less than for HDPE.

The long-time modulation experiments lead to a decrease in the apparent C_p at 292.9 K but remain still much higher than the expected value for the crystallinity of 28% at the same time and temperature. It is also considerably higher than for the 100% amorphous sample. Figure 5d summarizes the results. In the time domain, the dependence of the heat-flow rate suggests that the decrease in the apparent heat capacity is mainly due to crystal

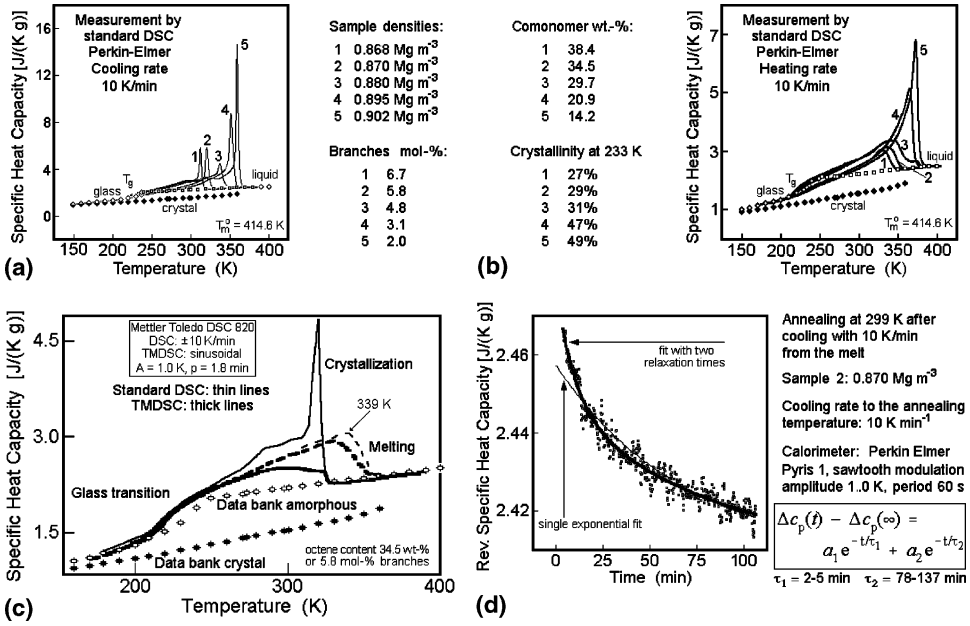

Figure 7. Apparent specific heat capacity of LLDPE, poly(ethylene-*co*-octene), measured by TMDSC (reversing C_p) and standard DSC (total C_p): (a) standard DSC traces on cooling of a series of polymers (the branches are calculated as moles of $=CH-C_6H_{13}$ per 100 backbone atoms); (b) standard DSC traces on subsequent heating of the series of polymers cooled from the melt in (a); (c) comparison of the apparent C_p by standard DSC and quasi-isothermal TMDSC on cooling, followed by heating for sample 2; (d) time dependence of the apparent reversing C_p on long-time quasi-isothermal analysis at 299 K (quasi-isothermal TMDSC of a sample cooled from the melt to 299 K, as in (a)).

perfection with time, which cannot be reversed on the subsequent heating and cooling cycles.

3.4. PE2M. Figure 6 gives the standard DSC and TMDSC results for PE2M. In Figure 6a heat-flow-rate curves by standard DSC are reproduced. On first heating, the fresh sample shows one major and two minor melting peaks. In the heating run after long-time annealing during the quasi-isothermal TMDSC on cooling, a similar curve is recovered. Crystallization on cooling at 5 K min^{-1} results in a single exotherm. It is interesting that in the subsequent heating PE2M starts the first melting at lower temperature and gives a melting peak at 290.3 K, followed immediately by a cold crystallization exotherm. After the completion of the cold crystallization, there appears a second melting with a shoulder and a major peak. Figure 6b illustrates the disappearance of the cold crystallization and the approach to the better crystallized samples in Figure 6a. The crystallinity deceases with increasing cooling rates and reaches 17.9% at 100 K min^{-1}. The data on cooling from 10 to 100 K min^{-1} are not shown in Figure 6b. They indicate no further change in the appearance of the heating trace, except for minor changes in the peak positions.

Figure 6c represents the comparison of standard DSC and quasi-isothermal TMDSC after crystallization on cooling at 5 K min^{-1}. A small shoulder at 291.0 K and a peak at 315.1 K characterize C_p(reversing). The shoulder, better seen in Figure 6d, is at the position of the first melting peak by standard DSC, while the peak is at the second melting peak. The cold-crystallization peak of the standard DSC trace is fully irreversible and does not show in TMDSC, neither does the 308.4 K shoulder in standard DSC appear in TMDSC.

Figure 6d contains an enlarged plot of the apparent reversing C_p by quasi-isothermal TMDSC of Figure 6c and the subsequent cooling and reheating runs. The end of the reversing melting after cooling at 5 K min^{-1} is at 323.1 K. In the cooling run, two reversing crystallization peaks appear, one at 299.1 K and one at 277.0 K, better seen in Figure 6e. The minimum between the two crystallization peaks is at 287.0 K. The onset of the crystallization is at 303.1 K. The supercooling for the crystallization under the given conditions, thus, is 20 K. After crystallization is complete, the cooling run matches the subsequent heating. The effect of the rate of cooling on C_p(reversing) is seen by comparison of the two melting experiments in Figure 6d. The sample cooled at 5 K min^{-1} has a much higher peak compared to the sample that underwent slow cooling with TMDSC. It is a common observation that faster crystallization yields higher reversing melting peaks.[24] The peak heights of the apparent C_p above the baseline of the liquid samples in Figure 6c are 1000 J K^{-1} mol^{-1} at 290.3 K and 1110 J K^{-1} mol^{-1} at 316.5 K for standard DSC, while TMDSC in Figure 6c,d results in 160 J K^{-1} mol^{-1} at 291.0 K and 320 J K^{-1} mol^{-1} at 315.1 K. The dotted lines in Figure 6d,e represent the baseline C_p of the amorphous sample, while the dashed lines are the heat capacity for crystalline PE2M without latent heat contributions. They were calculated by

$$C_p(\text{PE2M}) = 19C_p(\text{PE}) + C_p(\text{PIBUT}) \qquad (5)$$

where C_p(PE) and C_p(PIBUT) are the C_p of PE and polyisobutylene, PIBUT $[-C(CH_3)_2-CH_2]$.[36]

The long-time modulation experiments on cooling in Figure 6e show a decrease in the apparent C_p at 299.1 and 277.0 K, the peak temperatures in the cooling run of Figure 6d. A double-exponential fit of the data yields the ultimately constant level of reversible heat capacity, as shown in the figure. The reversible C_ps are still higher than the expected values for the remaining crystallinities at the given times and temperatures and also higher than C_p for the amorphous sample. The same tendency is seen at 275.0 and 317.1 K for the heating runs in Figure 6d. The time dependence of the heat-flow rates in the cooling experiment of Figure 6e is gained from Figure 6f at 299.1 K. The modulated portion of the heat-flow rate is superimposed on the irreversible crystallization from the melt which starts after the decrease of temperature to 299.1 K and lasts for about 30 min (compare to Figure 3f). The asymmetry of the upper and lower envelope of the modulation indicates that there is an additional exotherm of crystal perfection with a longer relaxation time. Before steady

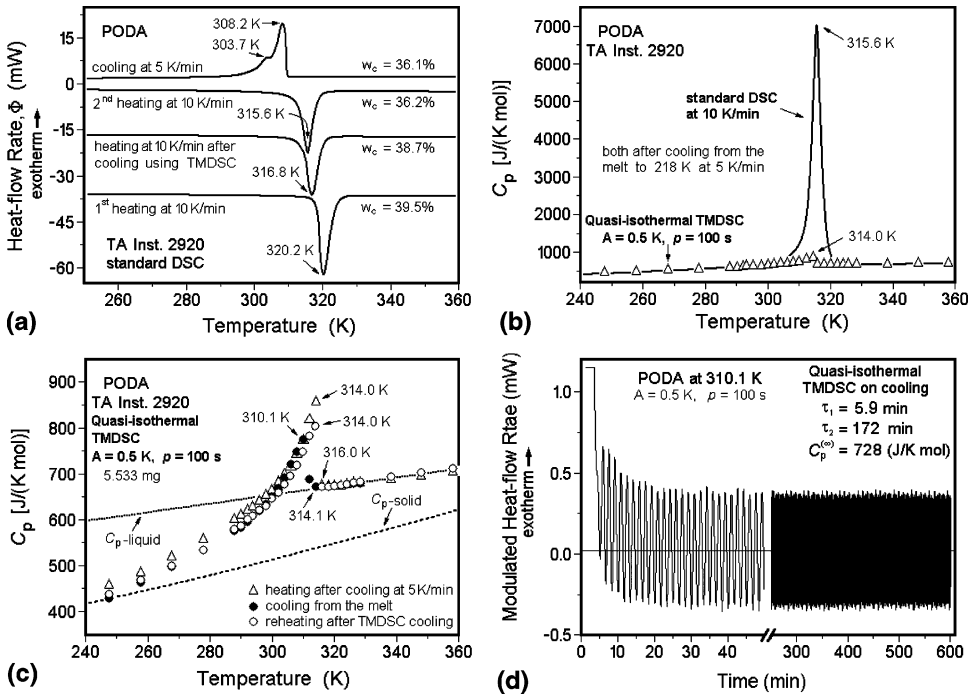

Figure 8. Results for PODA on standard DSC and quasi-isothermal TMDSC on heating, cooling, and reheating: (a) standard DSC traces; (b) comparison of C_p by standard DSC and quasi-isothermal TMDSC on heating after cooling at 5 K min^{-1} from the melt; (c) apparent, reversing C_p on stepwise heating, cooling, and reheating, measured by quasi-isothermal TMDSC; (d) time dependence of the apparent C_p on long-time quasi-isothermal analysis at the maximum of the cooling-run of (c) (compare to Figure 3d,f).

state is reached, the earlier exotherms in the modulated heat-flow rate decrease more than the subsequent endotherms of the heating cycle. This suggests that the decrease in the apparent heat capacity is mainly due to the crystal perfection with time which cannot be reversed in the heating cycle that follows.

3.5. LLDPE. The properties of LLDPE, poly(ethylene-*co*-octene), a PE with hexyl branches, were analyzed earlier.[8−10] A brief review of the extended data sets with standard DSC and TMDSC is represented in Figure 7. The standard DSC curves in Figure 7a illustrate the typical two-step crystallization seen on cooling, consisting of a sharp peak, followed by a slow further growth of crystals which stretches to the glass transition temperature. The slow crystallization at low temperature becomes the majority process with increasing branch content. Figure 7b illustrates the corresponding heating traces by standard DSC. With increasing branch content, the sharp portion of the melting peak disappears. The comparison between standard DSC and the quasi-isothermal TMDSC is shown for sample 2 in Figure 7c. On cooling, the crystallinity is 15% at 293 K and increases on further cooling to 29% at 233 K. A broad reversing melting peak at a temperature of about 334 K can be seen in Figure 7c with an increasingly smaller amount of reversing melting at the highest temperatures. At 334 K the apparent reversing C_p of the melting peak is estimated to be about 94% of the total C_p. The supercooling is large, about 30 K. Figure 7d, finally, shows the approach to fully reversible melting at longer times (compare to Figure 3d).

3.6. PODA. Poly(*n*-octadecyl acrylate), PODA, with a side chain of $-(CO)O(CH_2)_{17}CH_3$ was analyzed with standard DSC and TMDSC. Its chemical structure is given in Figure 1, and the T_ms of PODA and similar polymers with different structures and chain lengths are illustrated in Figure 2. The new thermal analysis results are presented in Figure 8. Figure 8a shows that the first heating (fresh sample) gives a melting peak at 320.2 K, in good accord with the wide spread of data in Figure 2, with a heat of fusion of $\Delta H = 99.6$ J g^{-1}, the second heating gives a melting peak at 315.6 K and a ΔH of 89.9 J g^{-1}, and the heating runs after cooling with quasi-isothermal TMDSC give a melting peak at 316.8 K and a ΔH of 96.1 J g^{-1}. In the cooling runs at 5 K min^{-1} from the melt, PODA shows a crystallization peak at 308.2 K and a shoulder at 303.7 K, with a ΔH of 88.4 J g^{-1}. The comparison between standard DSC and the quasi-isothermal TMDSC is shown in Figure 8b. The small reversing melting peak is located inside the melting peak of the standard DSC trace. The peak heights of the apparent C_p above the baseline of the liquid sample are 7028 J K^{-1} mol^{-1} at 315.6 K on standard DSC and 197 J K^{-1} mol^{-1} at 314.0 K in TMDSC. Figure 8c is an enlarged plot of reversing C_p, together with the results gained on cooling and on repeating of the quasi-isothermal experiment on heating after the prior cooling run. The dotted line is the baseline C_p of the liquid sample,[38] while the dashed line is the baseline of the solid given in the ATHAS Data Bank.[36] The reversing C_p after cooling at 5 K min^{-1} is higher than that on the slow quasi-isothermal cooling and reheating. The quasi-isothermal steps on cooling show a reversing crystallization peak at 310.1 K and an onset of crystallization at 314.1 K. The subsequent heating (open circles) reveals a reversing melting peak at 314.0 K with the end of melting at 316.0 K. Thus, the experimental supercooling of PODA is 2 K. Long-time modulation experiments give a continuing change in the apparent heat capacity as can be derived from Figure 8d. A double-exponential fit indicates a reversible apparent C_p of 728 J K^{-1} mol^{-1}, considerably higher than C_p for the liquid at the temperature, although the sample still had a ΔH of 75.1 J g^{-1} after 10 h annealing with quasi-isothermal TMDSC at 310.1 K. The time dependence of the heat-flow rate at 310.1 K is analogous to that of Figure 3f for HDPE.

3.7. X-ray Results. Figure 9 is a plot of the diffraction patterns in terms of the intensity vs 2θ for the newly analyzed samples. Figure 9 shows that the HDPE is an orthorhombic crystal (space group *Pnam*, chain direction along the *c* axis)

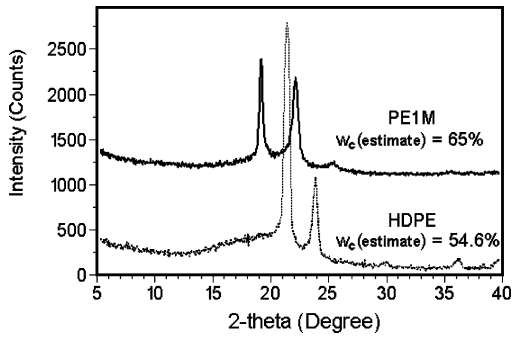

Figure 9. X-ray data of the precise PE copolymer PE1M with 20 CH_2 units per structural repeating unit compared to HDPE (for the structures, see Figure 1). Successive curves are displaced for clarity.

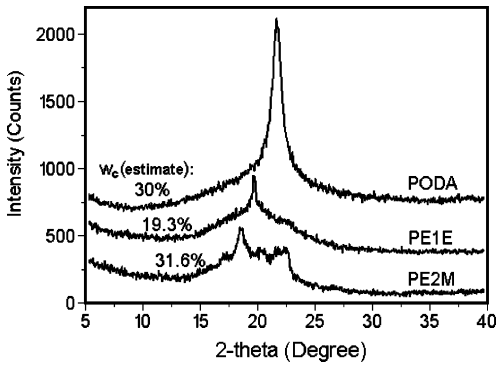

Figure 10. Comparison of X-ray data of PE2M, PE1E, and PODA with 20 chain atoms in the side chain of each structural repeating unit (for the structures, see Figure 1). Successive curves are displaced for clarity. Note that the intensity scale is expanded relative to Figure 9.

with its peak positions at 2θ of 21.4°, 23.8°, 29.8°, and 36.3° and relative intensities above the amorphous background of 100, 33, 2, and 4%. This corresponds to the original data by Bunn[39] for the 110, 200, 210, and 020 reflections of peak intensities of 100, 35, 1, and 5%, respectively.

The structure of PE1M in Figure 9 is typical for monoclinic polyethylene (space group *C*2/*m*, chain axis along the *b* axis) with the planes of the trans-conformations arranged in parallel. Earlier, the monoclinic lattice was indexed as a triclinic unit cell of half the size along *a*,[40] which loses the mirror plane normal to the chain direction.[41,42] The triclinic unit cell was also applied in a recent, more detailed analysis of the crystal structure and morphology of PE1M,[37] which will be discussed in section 4.2. The diffraction peaks are at 19.1, 22.1, and 25.6° with relative intensities of 100, 83, and 4.5%, compared to the monoclinic PE at 19.45, 23.17, and 25.11° with intensities of 100, 60, and 26% for the 100, 200, and $\bar{2}01$ reflections, respectively.[41,43] The shift of the 200 reflection to a smaller diffraction angle signifies a slightly larger unit cell. A similar effect was seen for the (orthorhombic) *a*-axis dimension of free-radical polymerized poly(ethylene-*co*-propylene)s.[44] Despite the fact that the methyl groups do not fit the PE crystal lattice, the copolymers with 5% methyl side groups showed a lattice expansion of 2.6−5.1%, which corresponds to a decrease in diffraction angle by 0.6°−1.2°, the same magnitude as seen in the monoclinic 200 reflection of PE1M. Experiments on a wide variety of branched samples led to the conclusion that a fraction of the methyl groups could be accommodated as defects within the crystal lamellae.[42]

The diffraction pattern for PE1E in Figure 10 shows only one diffraction peak at 19.6° and a broader shoulder at 22−23°, superimposed on a broad, amorphous background between 13° and 27° which is similar for all polymers in Figures 9 and 10. A sample crystallized somewhat better showed two scattering peaks: one at 18.7° shifted by 0.9° to a smaller angle and a much smaller one at 21.4°.[45] The triclinic 010 and 100 reflections of *n*-octadecane at 19.3° and 21.7° at relative intensities of 100 and 6%, respectively,[46] match these results. All 18 other diffractions of relative intensities above 5% identified in the paraffin are absent in PE1E. They are of the *hkl* type with $l \neq 0$ and involve the chain axis. For comparison, the hexagonal diffraction peak of PE at room temperature and atmospheric pressure is observed in drawn, gel-spun ultrahigh molar mass PE at about 20.5°.[47] The increase of the dimension of the orthorhombic *a*-axis due to the ethyl group in poly(ethylene-*co*-1-butene) is just below the broad range reported for the free radical copolymers with propene,[44] indicating less inclusion of ethyl groups than methyl groups into the PE crystal. A more open structure for the better crystallized sample would be able to accommodate some more ethyl side groups, thus making a triclinic structure tending to (pseudo)hexagonal possible for PE1E.

A completely different diffraction pattern arises from PE2M. The crystallinity seems to be somewhat larger than in PE1E. A series of small diffraction peaks can be seen in Figure 10. The diffraction peaks are located at (17.1°), 18.4°, (20.6°), 21.5°, and 22.5°, with the less prominent ones in parentheses. Most of these spacings can be found in the triclinic, orthorhombic, and hexagonal structures of the paraffins where they originate from the lateral packing in the chains.

The final pattern in Figure 10 is that of PODA. A single, strong diffraction-peak is seen at a 2θ of 21.6° on a broad, amorphous background. Again, the lattice spacing is similar to the well-known, strong 110 reflection of orthorhombic paraffins with similar odd numbers of CH_2 groups of 21.6°, but the 200 reflection at 24.0° is missing and should have a 50% relative intensity. All other diffractions of the up to 70 peaks identified in paraffins are of the *hkl* type with $l \neq 0$, involving the chain axis are absent in PODA. This is an indication of the absence of sufficiently well-defined lamellar surfaces at reasonable angles to the CH_2 chain segments of 2.5 nm length. Finally, the hexagonal structure of polyethylene has a diffraction angle of $2\theta = 20.5°$,[47] which would point to a slightly enlarged hexagonal unit cell for PODA.

A crystallinity estimate from the ratio of the crystalline to the total WAXD intensity over the measured range of 2θ is 54.5% for HDPE, 65.0% for PE1M, 19.3% for PE1E, 31.6% for PE2M, and 30% for PODA. Reported adjustment factors for the amorphous intensity of PE due to the limited diffraction range employed in the analysis vary between 1.2 and 0.9 and have been neglected because of the uncertainties that exist for the crystallinities derived from the heats of fusion to which the X-ray crystallinities should be compared and are shown in Figures 3−8a (first heating).

4. Discussion

4.1. The Three Limiting Materials HDPE, LLDPE, and Eicosane. The five macromolecules with precise chemical structures of Figure 1 have sequences of 20, 17, and 22 CH_2 groups along the backbone or as side groups. These sequences make up the crystallizeable units which are more or less decoupled from the overall macromolecule, which in all cases have a total of 2500−10 000 carbon atoms. Their crystal and phase structures as well as their transitions will be compared to the following three limiting materials to highlight the considerable differences:

The first of the limiting materials is HDPE, analyzed in Figure 3. It is a linear polymer with negligible branches. It crystallizes

orthorhombically (see Figure 9). The identical HDPE was crystallized at elevated pressure (>350 MPa) to an extended-chain macroconformation. After cooling and pressure release, the samples were close to equilibrium with a crystallinity of 98% and with lamellar thicknesses in direction of the chain of up to 3 μm.[48] In this morphology and macroconformation, the short molecules with lengths of less than 20 000 Da separated from the broad distribution of lengths according to a eutectic, multiphase diagram.[5−7] The extended-chain equilibrium crystals melt fully irreversibly.[7] On crystallization from the melt at atmospheric pressure, as in Figure 3, folded-chain crystal lamellae with a reduced crystallinity of only 70−80% result. A fold length of 15−20 nm is observed on crystallization at 390 K, which can extend on annealing at higher temperatures by as much as 10-fold.[49] The reversing melting in Figure 3 fits the earlier TMDSC results on different HDPEs which led to the picture of a globally metastable structure, made up of nano- to microphase crystals separated by amorphous areas. The longer molecules traverse the phase boundaries at points of decoupling where their crystalline thermodynamic nature changes from crystalline to amorphous.[23] At the growth face of the crystals, local equilibria were identified by TMDSC involving decoupled molecule segments which can avoid the need of molecular nucleation.[24] The specific reversible melting, defined by the ratio of the reversible enthalpy of fusion, measured by TMDSC, to the total, measured by standard DSC, starts in Figure 3b,c with values above 70% at about 330 K, but at these temperatures only small changes in crystallinity occur.[32] Approximating the specific reversible melting (per kelvin) by the ratio of excess reversible to total heat capacity, with the excess measured above the baseline of the semicrystalline sample, one can conclude that the main DSC melting peak and the reversing TMDSC melting peak both occur not far from the end of melting. At this temperature a large change in crystallinity occurs, and one finds from Figure 3b an estimate of 15% for the specific reversing melting. Considering the large uncertainties of the DSC melting peak because of instrument lag and the change of the reversing peak due to the reorganization, seen in Figure 3d, this value agrees well with the more detailed study of the specific reversibility of PE.[32] The supercooling of about 10 K is also in agreement with prior extensive studies on seeded and unseeded PE samples of the same lot as analyzed in this research.[29,35]

The LLDPE of Figure 7 represents the second limiting material as an example leading to poorer crystallization. Samples 1−3 in Figure 7 of these random copolymers have similar overall concentrations of branches to the precisely structured macromolecules, and thus a similar average CH_2 sequence length, but contained in a random distribution. Different from the HDPE is the distinct two-part crystallization in Figure 7a. A temperature-resolved X-ray study of sample 2 revealed a mixture of hexagonal and orthorhombic crystals.[10,50] The DSC and TMDSC results in Figure 7c illustrate that about half of the crystallinity has a broad melting region that reaches from the low-temperature beginning of the glass transition at 220 K to about 300 K. This portion melts largely reversibly with a specific reversibility of >75%[32] and represents mainly the fraction with hexagonal crystals[50] and, judging from the melting temperatures, must consist of shorter chain segments. The higher melting half of the crystallinity is orthorhombic, similar to the chain-folded crystals of HDPE, and its specific reversibility decreases to less than 50%.[32] The supercooling, when judged from the end of melting and beginning of crystallization by TMDSC in Figure 7c, has doubled compared to HDPE. The maximum of melting at 339 K corresponds to chain-folded crystals of LDPE with similar branch content, reviewed earlier and discussed with the models proposed at that time, including and excluding mixing terms.[51]

The third limiting material is represented by the fully decoupled sequences of paraffins of the same length as in *n*-$C_{20}H_{22}$, eicosane. The T_m can be seen in Figure 2 to be 311 K. The supercooling was observed to be less than 0.1 K when crystallized on cooling with a rate of 0.1 K min^{-1},[52] and TMDSC could prove full reversibility of melting and crystallization for *n*-paraffins of 60 chain atoms or less with a modulation amplitude of ±0.05 K.[27,29] All paraffins with odd numbers of chain atoms are orthorhombic, with a structure similar to polyethylene, while the even ones are triclinic up to *n*-$C_{24}H_{50}$ and monoclinic above.[53] These differences arise mainly from the need to pack the CH_3 end groups to obtain closely packed stacks of the chain molecules[54] and become unimportant for longer paraffins. The lateral packing of the paraffins can be described in terms of the arrangement of the planes of the zigzag chains. A parallel arrangement (| | |) is found for the triclinic and monoclinic molecules and a nonparallel one (\ / \) for the orthorhombic molecules. On disordering, all three tend to a more or less pseudohexagonal structure,[54] as is seen also in the condis phases,[55] stable a few degrees below the melting temperatures for paraffins up to $C_{44}H_{90}$. The thermal properties of all these paraffins have been reported earlier.[56]

4.2. Crystal and Phase Structure. The study of the crystal structures in Figures 9 and 10 gives the result that the top four macromolecules in Figure 1 do not have an orthorhombic structure which is the stable structure of PE and the odd-numbered paraffins at room temperature. The molecule which comes closest to a PE crystal structure is the monoclinic PE1M with the smallest branch length. An extensive and more precise study of an identical PE1M, crystallized from solution and melt by wide- and small-angle X-ray diffraction and electron diffraction, was published recently[37] and agrees with the data presented here but discusses the results in the older triclinic setting for PE,[40] discussed earlier.[42] Both PODA and PE1E show a single strong diffraction peak and appear to be related to the pseudohexagonal PE or paraffins with (100) reflections at 20.5°. The PODA has a larger diffraction angle (21.6°), indicating a closer packing which tends toward the paraffinic orthorhombic structure, while the PE1E has a smaller angle (18.7°−19.6°), indicating an expanded lattice tending toward the paraffinic triclinic structure. The PE2E, in turn, seems to be able to exist simultaneously at least in two different paraffinic structures.

To judge crystallinity, ease of crystallization, and crystal morphology, one must compare Figures 3a−8a. The crystallinity is calculated with the orthorhombic heat of fusion because the heats of fusion and the change with temperature of the other crystal structures are not as well established. The heat of fusion of the monoclinic and triclinic structures of paraffins is only little less than that of the orthorhombic crystals, while the heat of fusion of the disordered, pseudohexagonal phase is always smaller, variable, and may be as little as 50% of the heat of fusion of the orthorhombic crystals.[55,57] In comparing the crystallinity from X-ray diffraction and heat of fusion, one might assume, thus, that the former should always be larger, but two other points limit such interpretation. The X-ray diffraction often misses nanocrystals which can still yield a sizable heat of fusion, and slow and fast cooling followed by annealing, even at room temperature, can yield largely different crystallinities; i.e., the different experiments may refer to samples of different histories. The small samples on hand did not allow for more extensive experimentation.

The ease of crystallization is judged for this comparison by the difference between the (first) crystallization peak reached on the cooling at 5 K min^{-1} and the (corresponding) melting peak on subsequent heating at 10 K min^{-1}. The two polyethylenes with folded-chain crystals, HDPE and LLDPE, have the largest differences between crystallization and melting peak (17 and 20 K, respectively). The PE1M, PODA, PE1E, and PE2M with crystallinities (by DSC) of 46, 36, 27, and 20%, respectively, have differences of only 8.5, 7.4, 4.1, and 5.9 K, respectively. The highest DSC melting peaks of HDPE, LLDPE, PE1M, PODA, PE1E, and PE2M are at 409, 339, 338, 320, 309, and 320 K, respectively. Thus, one can distinguish the slower crystallization with standard chain-folding from the crystallization of the precisely segmented macromolecules.

A comparison to the fully decoupled paraffin eicosane with a T_m of 311 K and a chain length of ≈2.5 nm reveals the following: There is a correlation to the T_m of eicosane for PODA, PE1E, and PE2M, but not for LLDPE and PE1M. For LLDPE, this is linked to the PE-like crystallization of the longer CH_2 sequences which are always present in random copolymers.[1−3] For PE1M, the higher melting peak temperature and crystallinity are most likely due to the changes in crystal perfection due to easier inclusion of methyl branches within the crystal, variations in the surface free energies, and differences in the annealing histories, enhanced by the different degrees of initial supercooling. The inclusion of methyl groups is in accord with the increased lattice dimensions[44] and more extensive data on structure and morphology,[37] discussed below. The lower crystallinities of PE1E and PE2M may be coupled to the distinctly lower supercooling which yield a lesser driving force toward crystal perfection on crystallization. For PE2M, one can see in Figure 6a,b that reorganization is sufficiently slow that on second heating the crystals grown on cooling at faster rate than 1.0 K min^{-1} melt almost completely on heating before recrystallization by cold crystallization. Finally, it should be noted that there is no similarity of any of the samples to the 100% crystallinity of eicosane and its reversible crystallization without supercooling.[27]

The crystal size in the chain direction of HDPE and also for the longer CH_2 sequences in LLDPE is set by the chain-folding. The fraction of crystals in LLDPE which melts at low temperature, in contrast, must be governed by the random occurrence of branch points and corresponds to a broad distribution of sequence lengths, in agreement with the broad melting range in Figure 7c. For PE1M, an electron microscopic study of the morphology of crystals from solution and melt is available from the work of Lieser et al.[37] Both crystallization types resulted in laterally micrometer-sized lamellae of a thickness in the chain direction of 10−20 nm which is supported by low-angle X-ray diffraction peaks related to a repeat distance of 16.4 nm. Since the molar mass of PE1M is identical to the present samples, the molecules are of an average zigzag length of 183 nm, i.e., require chain-folding. The extended-chain sequence length of 21 C atoms for defect-free crystallization, however, is only 2.7 nm. The lamellae, thus, must either include the methyl branches within the crystals and collect the amorphous phase at the top and bottom surfaces of the lamellae as a whole or consist of multiple crystal layers with methyl branches collected between the layers. Making use of the innermost X-ray-diffraction peaks at 3°−10°, not distinguishable in Figure 9, a unit cell with a repeat of $c = 5.3$ nm was derived which is identical to the *b*-axis in the here assumed monoclinic lattice and accounts for a unit cell length of two repeating units (i.e., a length of *n* equal to four in Figure 1). This makes it likely that the methyl groups are included in the crystals, but collected in defined defect planes,[37] different from the randomly branched copolymers.[44,51]

A similar structure was found earlier in the mesophase-forming poly(4,4′-phthaloimidobenzoyl-*n*-methyleneoxycarbonyl)s, PEIM-*n*, where *n* designates the number of methylene groups in the repeating unit. The chemical structure for PEIM-22 is given in Figure 1. Calorimetric as well as X-ray data are available for PEIM-22,[58,59] while supporting solid-state NMR information is available PEIM-9 and PEIM-12.[60,61] These precisely segmented PEIMs have a smectic-like layer structure with a coherently scattering stack of 3−4 repeating units,[59] with the methylene sequences being nanophase-separated in a hexagonal condis structure with specific bonds ordered into a trans conformation.[60,61] In these and similar segmented macromolecules the two chemically different segments are at the basis of the nanophase separation, driven by the immiscibility of the two sequences. The crystallinity of the CH_2 sequences provide the largest portion of the heat of crystallization and stabilize the overall crystal stacks, which in turn assume the lamellar superstructure.[1] The PE1M seems to take a similar structure with the separation occurring with the smallest possible difference in geometry. The defect planes of $CH-CH_3$ groups with surrounding chain defects are too small to be acting as a separate phase but are sufficient to act as a point of decoupling which affects the phase transition. With increasing sequence lengths, the structures extend to the better-known block copolymers in which the size scale is expanded to microphases. Again, for the phase separation one expects a lamellar superstructure for these blocks of mole fraction 0.5, not due to a need to chain-fold but due to the need to place the points of decoupling at the interface. The lamellar superstructure will affect the crystal morphology as soon as it approaches the fold length of the crystallizable sequence(s), which can be affected to some degree by the crystallization temperature.[62] The present samples and the PEIMs extend this continuous change in alternating chemical structure to a length scale smaller than the fold length and illustrate the overriding macromolecular effect of chain folding being maintained by segmentation within the lamellar superstructure without complete loss of the overall crystalline order.

It is interesting to see that chain-folding of sequences without decoupling seems to be the reason for the slower crystallization kinetics of HDPE and LLDPE. The crystal fraction in LLDPE which grows and melts at low temperature is again different from the macromolecules with precise sequence lengths. On heating, it melts over a wide temperature range, reaching from the beginning of the glass transition into the region of melting of the longer sequences, while PE1M, PODA, PE1E, and PE2M (after sufficient reorganization) can crystallize and melt much more sharply.

4.3. Heat Capacity and Glass Transition. The low-temperature heat capacities of all solid polymers from pure polyethylene to copolymers and paraffins could be represented by their constituent vibrational spectra. For the liquid states, the contributions from the large-amplitude motion and the larger external contribution ($C_p - C_v$) have to be added to the vibrational heat capacity and give a similarly good fit.[1,15,17,38,56] The heat capacities and their use in the extrapolations as baselines can be seen in Figures 3−8. Next, with the help of TMDSC, it is possible to separate the thermodynamic heat capacity in eq 2 from the latent-heat effects. The reversible latent heats are more difficult to assess than the irreversible ones, as will be discussed in section 4.4.

Figure 3b suggests equal apparent heat capacities up to about 360 K for HDPE from DSC and TMDSC. The enlarged scale in Figure 3c indicates that a gradual increase in heat capacity beyond the 100% crystalline, solid value starts at 230 K. This

is the beginning (of the major portion) of the glass transition.[13] The HDPE reaches the end of the glass transition of a sample with 70% crystallinity only at about 290 K, typical for the broadening seen in semicrystalline PEs.[1] There is no indication in PE and any other of the here analyzed macromolecules of an additional step in the glass transition which could indicate an amorphous fraction that remains rigid to higher temperature (RAF).[1] The LLDPE in Figure 7c reveals that melting has started already at 230 K, the beginning of the glass transition, and continues with increasing contribution to the latent heat. The low-temperature melting is fully reversible. The eicosane used as the third limiting substance in this discussion is 100% crystalline and has no glass transition outside the melting region, but note it has a gauche−trans contribution to the heat capacity within the crystal,[56] as is also observed for all other PEs and aliphatic polyoxides.[1,63]

The four precisely segmented macromolecules also have glass transitions which begin, as in PE, at about 230 K and are broadened due to the crystallinity. For PE1M, PE1E, PE2M, and PODA the upper ends of the glass transitions are at 270, 265, 265, and 280 K, respectively, with a continuation of the increase in reversing heat capacity due to melting without noticeable break (see Figures 4−6 and 8). The materials with the highest crystallinity (PE1M and PODA) have the most broadened glass transitions, but overall the broadening is less than in PE, suggesting less stress transfer from crystals to amorphous phases. Calorimetry of PEIM-22 of Figure 1 also showed a gradual beginning of the glass transition with an end of the transition at about 325 K. From the change in C_p at the midpoint of the glass transition (at 317 K), it was concluded that the higher T_g was due to condis crystals contributing to the vitrification.[58]

4.4. Melting by TMDSC. The study of the response to temperature modulation as a function of increasing and decreasing base temperature T_0, shown in Figures 3−8, permits some additional insight into the nature of the crystals. Initially, one might have expected to see almost full decoupling of the crystallized segments at the amorphous interface. This would have led to fully reversible melting as in eicosane and all decoupled segments shorter than 75 CH_2 groups,[29] i.e., including all copolymers discussed in this paper. This is clearly not so. The macromolecular nature still influences the crystals and does not permit full reversibility. Comparing the DSC and TMDSC amplitudes at their respective peak temperatures, as given in Figures 4−6 and 8, led for the better crystallizing PODA and PE1M to a reversing amplitude of 3.0 and 6.7%, respectively. For the poorer crystals of PE1E and PE2M, the reversing amplitudes are 21 and 29%, respectively. The better the crystallization, the lower is the reversing fraction, as was observed for many other polymers.[24] The same analysis for HDPE in Figure 3b and LLDPE in Figure 7c yields 15 and 75%, respectively. Comparing these numbers leads to the possibility that crystal perfection is the most important factor governing the reversing melting behavior. The best crystals in PODA and PE1M may not show any reversibility, as is also seen in extended-chain crystals of polyethylene and poly(oxyethylene)[24] and sharply folded crystals of poly(oxyethylene).[63]

Comparing the overall supercooling between the last noticeable reversing melting and the first reversing crystallization on cooling by TMDSC, as quoted in the Results section, to the differences between cooling and heating peak temperatures by standard DSC, quoted in the discussion of the phase structure, shows some interesting differences. The three samples of poorest crystals—LLDPE, PE1E, and PE2M—show a larger supercooling by TMDSC (30, 8, and 20 K) than by DSC (20, 4.1, and 5.9, respectively). The three other samples (HDPE, PODA, PE1M) show a smaller supercooling by TMDSC (10, 2, and 2 K, respectively) than by DSC (17, 7.4, and 8.5 K, respectively). The answer for these differences lies in the amount of reorganization and recrystallization which occurred in the samples after initial crystallization and on the slow heating in the TMDSC experiment. The initially poorer crystals move the melting to higher temperature than the initially better crystals. In fact, the PODA and PE1M come close to the originally expected zero supercooling of paraffins, expected by TMDSC, but the crystallization rate is sufficiently slow that no substantial amounts of crystals grow or melt under the time constraints of the experiments.

The poorer crystals of PE1E and PE2M in Figures 5 and 6 show multiple crystallization and melting peaks, indicative of multiple improvements or crystal structures. As seen earlier, cold crystallization does not have a reversing component[24] and also does not show any in Figure 6c. The multiple melting peaks in Figures 5b,c and 6c have only barely noticeable reversing components; i.e., they also connect to mainly irreversible processes.

For the TMDSC of cooling and subsequent heating of PE2M in Figure 6d, two reversing peaks are observed. The first peak involves the main crystallization on slow cooling, as is obvious from Figure 6f which illustrates the underlying irreversible crystallization. The starting temperature of crystallization is at 303.1 K and defines the above-mentioned supercooling of 20 K. The second peak starts at 287 K, a much larger supercooling of 36 K. The total crystallization was assessed by standard DSC after the quasi-isothermal TMDSC on cooling to various temperatures. At 299 K, the temperature of the first peak in reversing crystallization in Figure 6d, the crystallinity had reached 10%, much more than estimated from the area of the reversing peak (<1%). Between the two peaks, at 287 K it reached 20%, and at the second peak, at 277 K, it was 20.5%. At the end of the second peak, at 269 K, the crystallinity was 21.6%, and at 217 K, the 31.5% shown in Figure 6a was reached. These runs yield an increase in crystallinity by 1.6% throughout the temperature range of the second reversing peak, but from the peak area in Figure 6e, which is the order of magnitude of 0.5%, one can estimate that most of this increase in crystallinity is still irreversible. The special observation is that some small changes at similar temperatures show also in the heating traces of Figure 6a,d. One concludes that on faster cooling crystallization occurs only at 36 K, supercooling into a low-temperature crystal form, which on second heating at 10 K min^{-1} melts at 290.3 K, undergoes cold crystallization, and finally melts at 316.5 K. On annealing at low temperature, most of the low-temperature crystals reorganize to a melting peak of 316−320 K. The reversing fraction of these crystals, however, remains, and an intermediate reorganization at 290 and 310 K is also visible in DSC and TMDSC traces. This complicated multiphase behavior on crystallization and melting is in accord with the overlap of diffraction patterns seen in Figure 10. Additional studies on larger samples with different histories are necessary to assign different structures to the various melting peaks.

The time scales of the reversing changes in latent heat in the TMDSC experiments are typically 2−25 min for τ_1 and 80−250 min for τ_2. The fast relaxation times are governed by the kinetics of melting and crystallization (and contributions of the recovery from the calorimeter lag), while the longer relaxation

times are indicative of the continuing reorganization at the chosen T_0 and crystal improvements which may occur on the reversing recrystallization. Once a crystal segment is completely melted, i.e., has lost its molecular nucleus or has improved its crystal to a sufficiently higher melting temperature, it will not participate in the subsequent modulation cycles. Again, more details can be extracted by combining specific samples with modulation experiments of changing frequency and amplitude.

5. Conclusions

By comparing macromolecules with precisely synthesized lengths of crystallizable units to a homopolymer and a random copolymer, new insight was gained into the nature of crystallization, melting, and the decoupling of sequences of 20 CH_2 groups. First, it was documented that their melting temperature is in the vicinity of T_m of the corresponding *n*-alkane, about 80−100 K below the melting temperature of the homopolymer. Within the variation given, this decrease is independent of the crystallinity and type of crystal and approximately applies even to the broad peak temperature of the LDPE and LLDPE with only an average chain length of the crystallizable units. The entropy effect of mixing and demixing of the defects along the chain seem to play a much smaller role than the crystal size. The sharpness of the melting, however, is directly linked to the precision of the chain segment lengths. The random LLDPE has a continuous melting without a major peak, covering about 150 K, while, after slow cooling, the samples of precise sequence lengths have their main melting occur over 10−25 K, compared to the homopolymer HDPE with a breadth of about 35 K.

The well-defined orthorhombic crystal structure of HDPE is not found for the sequences of CH_2 groups, but all have a more or less defect paraffin-like lateral packing. The PE1M is monoclinic, PODA is pseudohexagonal (to orthorhomic), PE1E is pseudohexagonal (to triclinic), LLDPE and PE2M have more than one crystal structure (orthorhombic + hexagonal and triclinic + hexagonal(?), respectively). The PEIM-22 also has two crystal structures, both with X-ray diffraction patterns which arise from both the ester−imide and alkane segments, with the alkane segment being largely hexagonal. Better crystallized sequences seem to be able to include some of the smaller branch units by increasing the unit cell dimensions. All samples remained semicrystalline and retain on slow crystallization 40−65% of the crystallinity of HDPE (≈75%). For PEIM-22 and PE1M, a sublayer structure was proven, separating a lamellar superstructure from 3 to 4 layers of alkane (condis) crystals.

The decoupling between the sequences along the backbone or from backbone to side group thus may have to be distinguished into decoupling at the surface of the lamellar fold surface superstructure and the internal layers after every 18−22 CH_2 sequence. The fold surface is linked to the macromolecular nature of the overall molecule and the internal surface to the analogous paraffin. The crystals are thermodynamically decoupled from the amorphous segments, but the points of decoupling transmit strains due to restrictions of volume and conformation, as is documented by the glass transition and its broadening to higher temperature. The internal decoupling within the crystals, proven at present only for PE1M, must cause the lowering of the melting temperature to T_m of the fully decoupled paraffins. The sharply segmented polyethylenes, however, have not gained the reversibility of melting seen in the paraffins. For the flexible CH_2 chains, no rigid-amorphous fraction is observed.

The coupling to the amorphous phase preserves the macromolecular nature and strongly affects the supercooling and rate of crystallization and also slows the reorganization. There is much less supercooling in the precisely structured materials with less hindered points of coupling (2.0 K for PODA and PE1M) relative to the HDPE and LLDPE (10 and 30 K, respectively). In fact, this small supercooling approaches the reversibility of the analogous paraffin. Increasing the hindering, as in PE1E and PE2M, this supercooling increases to 8 and 20 K, respectively. The effect of the microstucture on the supercooling is obvious from this comparison. Adding the time effect by estimating the supercooling at a fixed cooling rate of 5 K min^{-1} followed by heating at 10 K min^{-1}, the microstructure is even more important. The supercooling increases for most samples on the faster cooling, but for PE2M it decreases drastically to 5.9 K due to the crystallization of a lower-melting crystal polymorph. For PE1E and LLDPE it decreases moderately to 4.1 and 20 K, respectively, due to reduction of the crystal perfection during heating.

The small amount of reversible melting, common in melt-crystallized homopolymers, is less in the precisely segmented polymers and approaches zero for the best crystallized samples, PODA and PE1M, estimated at 3 and 6.7% when compared to the HDPE (15%). The same was seen for sharply folded and extended-chain crystals. Having proven earlier that the main reversible melting occurs on the growth faces, this work seems to indicate that the points of decoupling of the crystallized segments are located at the surface and planes of defects which cut through the molecular chains. If there is no surface that is traversed by the molecules, as in extended-chain crystals and sharply folded crystals, there is no reversible melting beyond the limit of ≈75 chain atoms. In the present case both sequence ends may become sufficiently mobile on melting to lose their points of decoupling so that the sequence is fully removed from the crystal surface and must be newly nucleated to regrow on the cooling portion of the modulation. Since the supercooling is in all cases still larger than the ±0.5 K modulation and the crystallization is much slower at low supercooling than the melting on small superheating, the melting remains still largely irreversible, moving the length of reversible melting to much shorter chain length.

The larger amounts of reversible melting seen for LLDPE, PE2M, and PE1E, estimated to be 75, 30, and 21%, respectively, may be due to the much shorter sequences in LLDPE melting at low temperature and the existence of more effective points of decoupling in all three polymers.

Overall, it is concluded that the precise microstructure, the phase structure, and the intrinsic slowing of diffusion to and from the crystallization site in macromolecules need to be understood to interpret the differences of the analyzed samples. For a thermodynamic description, the nature of the points of decoupling which may lie on the surface of a lamellar superstructure or within the crystals must be established. At least for PE1M (and PEIM-22) both are present. Similar structures are likely for PODA, PE1E, and PE2M, although their defect planes would be more strained.

Acknowledgment. The work at the University of Tennessee at Knoxville and the University of Florida at Gainesville was supported by the Division of Materials Research, National Science Foundation, Polymers Program, Grants DMR-0312233 and 0314110, respectively. Support and use of equipment and laboratory space was provided by the Division of Materials Sciences and Engineering, Office of Basic Energy Sciences, U.S. Department of Energy at Oak Ridge National Laboratory, managed and operated by UT-Battelle, LLC, for the U.S.

Department of Energy, under Contract DOE-AC05-00OR22725. We thank Dr. Xiaoyun Ling of the Central X-ray Facility at UTK for the measurements displayed in Figures 9 and 10.

References and Notes

(1) Wunderlich, B. *Thermal Analysis of Polymeric Materials*; Springer-Verlag: Berlin, 2005.
(2) Mathot, V. B. F., Ed. *Calorimetry and Thermal Analysis of Polymers*; Hanser Publishers: Munich, 1993.
(3) Mathot, V. B. F.; Scherrenberg, R. L.; Pijpers, T. F. J.; Engelen, Y. M. T. Structure, Crystallization and Morphology of Homogeneous Ethylene-propylene, Ethylene-1-butene and Ethylene-1-octene Copolymers with High Comonomer Contents. In Hosoda, S., Ed. *New Trends in Polyolefin Science and Technology*; Trivandrum: India; 1996; pp 71−124.
(4) Smith, J. A.; Brzezinska, K. R.; Valenti, D. J.; Wagener, K. B. *Macromolecules* **2000**, *33*, 3781.
(5) Prime, R. B.; Wunderlich, B. *J. Polym. Sci., Part A-2* **1969**, *7*, 2061, 2073.
(6) Prime, R. B.; Wunderlich, B.; Melillo, L. *J. Polym. Sci., Part A-2* **1969**, *7*, 2097.
(7) Pak, J.; Wunderlich, B. *J. Polym. Sci., Part B: Polym. Phys.* **2002**, *40*, 2219.
(8) Androsch, R. *Polymer* **1999**, *40*, 2805.
(9) Androsch, R.; Wunderlich, B. *Macromolecules* **1999**, *32*, 7238.
(10) Androsch, R.; Wunderlich, B. *Macromolecules* **2000**, *33*, 9076.
(11) Dole, M.; Hettinger, W. P., Jr.; Larson, N. R.; Wethington, J. A., Jr. *J. Chem. Phys.* **1952**, *20*, 781.
(12) Wunderlich, B.; Dole, M. *J. Polym. Sci.* **1957**, *24*, 201.
(13) Gaur, U.; Wunderlich, B. *Macromolecules* **1980**, *13*, 445.
(14) Wunderlich, B.; Czornyj, G. *Macromolecules* **1977**, *10*, 906.
(15) Gaur, U.; Wunderlich, B. *J. Phys. Chem. Ref. Data* **1981**, *10*, 119.
(16) Wunderlich, B. *J. Chem. Phys.* **1962**, *37*, 1207.
(17) Bu, H. S.; Aycock, W.; Wunderlich, B. *Polymer* **1987**, *28*, 1165.
(18) Wunderlich, B.; Baur, H. *Fortschr. Hochpolymeren Forsch. (Adv. Polym. Sci.)* **1970**, *7*, 151.
(19) Wunderlich, B. *J. Phys. Chem.* **1965**, *69*, 2078.
(20) Arakawa, T.; Wunderlich, B. *J. Polym. Sci., Part C* **1967**, *16*, 653.
(21) Boller, A.; Jin, Y.; Wunderlich, B. *J. Therm. Anal.* **1994**, *42*, 307.
(22) Wunderlich, B.; Jin, Y.; Boller, A. *Thermochim. Acta* **1994**, *238*, 277.
(23) Wunderlich, B. *J. Polym. Sci., Part B: Polym. Phys.* **2004**, *42*, 1275.
(24) Wunderlich, B. *Prog. Polym. Sci.* **2003**, *28*, 383.
(25) Flory, P. J. *Principles of Polymer Chemistry*; Cornell University Press: Ithaca, NY, 1953.
(26) Wunderlich, B. *Macromolecular Physics*; Academic Press: New York, 1980; Vol. 3, discussed on pp 325−331.
(27) Pak, J.; Wunderlich, B. *J. Polym. Sci., Part B: Polym. Phys.* **2000**, *38*, 2810.
(28) Magonov, S. N.; Yerina, N. A.; Ungar, G.; Reneker, D. H.; Ivanov, D. A. *Macromolecules* **2003**, *36*, 5637.
(29) Pak, J.; Wunderlich, B. *Macromolecules* **2001**, *34*, 4492.
(30) Bassett, D. C.; Olley, R. H.; Sutton, S. J.; Vaughan, A. S. *Polymer* **1996**, *37*, 4993.
(31) Pak, J.; Wunderlich, B. *Thermochim. Acta* **2004**, *421*, 203.
(32) Androsch, R.; Wunderlich, B. *J. Polym. Sci., Part B: Polym. Phys.* **2003**, *41*, 2157.
(33) Gmelin, S. M. E.; Höhne, G. W. H.; Cammenga, H. K.; Hemminger, W.; Eysel, W. *Thermochim. Acta* **1994**, *247*, 129.
(34) Ishikiriyama, K.; Wunderlich, B. *J. Therm. Anal.* **1997**, *50*, 337.
(35) Wunderlich, B.; Cormier, C. M. *J. Phys. Chem.* **1966**, *70*, 1844.
(36) web.utk.edu/∼athas/databank; see also refs 15−17.
(37) Lieser, G.; Wegner, G.; Smith, J. A.; Wagener, K. B. *Colloid Polym. Sci.* **2004**, *282*, 773.
(38) Gaur, U.; Lau, S. F.; Wunderlich, B. B.; Wunderlich, B. *J. Phys. Chem. Ref. Data* **1982**, *11*, 1085.
(39) Bunn, C. W. *Trans. Faraday Soc.* **1939**, *35*, 482.
(40) Turner-Jones, A. *J. Polym. Sci.* **1962**, *62*, S53.
(41) Seto, T.; Hara, T.; Tanaka, K. *Japan. J. Appl. Phys.* **1968**, *7*, 31.
(42) Wunderlich, B. *Macromolecular Physics;* Academic Press: New York, 1973; Vol. 1, see Sections 2.3.6 and 2.4.1.
(43) Russel, K. E.; Hunter, B. K.; Heyding, R. D. *Polymer* **1997**, *38*, 1409.
(44) Martinez de Salazar, J.; Baltá Calleja, F. J. *J. Cryst. Growth* **1980**, *48*, 283; discussed also in Section 2.4.8, Figure 2.60 of refs 42 and 51.
(45) Sworen, J. C. Thesis, Department of Chemistry, University of Florida, Gainesville, FL, 2004.
(46) Muller, A.; Lonsdale, K. *Acta Crystallogr.* **1948**, *1*, 129.
(47) Uehara, H.; Kanamato, T.; Kawaguchi, A.; Murakami, S. *Macromolecules* **1996**, *29*, 1540.
(48) Geil, P. H.; Anderson, F. R.; Wunderlich, B.; Arakawa, T. *J. Polym. Sci., Part A* **1964**, *2*, 3707.
(49) Derived from the nine extensive sets of experiments, summarized in Figure 3.13 of ref 42.
(50) Androsch, R.; Blackwell, J.; Chvalun, S. N.; Wunderlich, B. *Macromolecules* **1999**, *32*, 3735.
(51) Wunderlich, B. *Macromolecular Physics*; Academic Press: New York, 1980; Vol. 3, Sect. 10.3.1.1, pp 275−288 and Figures X.8−12.
(52) Kraak, H.; Sirota, E. B.; Deutsch, M. *J. Chem. Phys.* **2000**, *112*, 6872.
(53) Broadhurst, M. G. *J. Natl. Bur. Stand.* **1969**, *65*, 1749, 1767.
(54) Kitaigorodsky, A. I. *Molecular Crystals and Molecules*; Academic Press: New York, 1973; pp 55−62.
(55) Wunderlich, B.; Möller, M.; Grebowicz, J.; Baur, H. *Conformational Motion and Disorder in Low and High Molecular Mass Crystals*; Springer: Berlin, 1988; Vol. 87, pp 44−50.
(56) Jin, Y.; Wunderlich, B. *J. Phys. Chem.* **1991**, *95*, 9000.
(57) Kwon, Y. K.; Boller, A.; Pyda, M.; Wunderlich, B. *Polymer* **2000**, *41*, 6237.
(58) Kwon, Y. K.; Pyda, M.; Chen, W.; Wunderlich, B. *J. Polym. Sci., Part B: Polym. Phys.* **2000**, *38*, 319.
(59) Kwon, Y. K.; Annis, B. K.; Chen, W.; Wunderlich, B. *J. Polym. Sci., Part B: Polym. Phys.* **2000**, *38*, 611.
(60) Chen, W.; Pyda, M.; Habenschuss, A.; Londono, J. D.; Wunderlich, B. *Polym. Adv. Technol.* **1997**, *8*, 747.
(61) Cheng, J.; Jin, Y.; Chen, W.; Pardey, R.; Cheng, S. Z. D.; Wunderlich, B. *Polym. Adv. Technol.* **1999**, *10*, 501.
(62) Zhu, L.; Cheng, S. Z. D.; Thomas, S. L.; Lotz, B. *J. Am. Chem. Soc.* **2000**, 5957.
(63) Qiu, W. L.; Pyda, M.; Nowak-Pyda, E.; Habenschuss, A.; Wunderlich, B. *Macromolecules* **2005**, *38*, 8454.

MA052010W